Functional Characterization of a Candidate Tumor Suppressor Gene, *Mirror Image Polydactyly 1,* in Nasopharyngeal Carcinoma

Merrin Man Long Leong[1], Arthur Kwok Leung Cheung[1], Tommy Chin Tung Kwok[1], and Maria Li Lung [1,2,#]

[1]*Department of Clinical Oncology, University of Hong Kong, Hong Kong (Special Administrative Region), People's Republic of China;*

[2]*Centre for Nasopharyngeal Carcinoma Research, University of Hong Kong, Hong Kong (Special Administrative Region), People's Republic of China*

#Corresponding author: Maria Li Lung

Address: Department of Clinical Oncology, The University of Hong Kong, Room L6-43, 6/F, Laboratory Block, Li Ka Shing Faculty of Medicine Building, 21 Sassoon Road, Pokfulam, Hong Kong

Tel: +852 39179783; Fax: +852 28166279; Email: mlilung@hku.hk

Novelty & Impact Statements:

Mirror Image Polydactyl 1 (MIPOL1) was initially known to be associated with congenital anomalies. Using functional approaches, it was found to be a tumor suppressor candidate gene in nasopharyngeal carcinoma (NPC). This current study provides strong evidence of the role *MIPOL1* plays as a tumor suppressor in NPC. It inhibits malignant cell migration, invasion, and metastasis through down-regulation of cancer-related signaling pathway members, hence, suggesting new therapeutic targets for NPC.

Abbreviations:

2D = 2-dimensional; 3D = 3-dimensional; AAALAC = Associating for Assessment and Accreditation of Laboratory Animal Care; AoE = Area of Excellence; Co-IP = co-immunoprecipitation; EBV = Epstein-Barr virus; ECM = extracellular matrix; FBS = fetal bovine serum; GAPDH = glyceraldehyde 3-phosphate dehydrogenase; H&E = hematoxylin and eosin; IS = intrasplenic; LOH = loss of heterozygosity; MIPOL1 = mirror image polydactyl 1; MMCT = microcell-mediated chromosome transfer; MMPs = matrix metalloproteinases; M-MLV = Moloney Murine Leukemia Virus; NCS = newborn calf serum; NPC = nasopharyngeal carcinoma; RTKN = Rhotekin; S.E.M. = standard error mean; TSG = tumor suppressor gene; VA = vector alone; WT = wild type; Y2H = yeast two-hybrid.

Abstract:

Mirror Image Polydactyl 1 (MIPOL1) is generally associated with congenital anomalies. However, its role in cancer development is poorly understood. Previously, by utilizing the functional complementation approach, microcell-mediated chromosome transfer (MMCT), a tumor suppressor gene, *MIPOL1*, was identified. *MIPOL1* was confirmed to be down-regulated in nasopharyngeal carcinoma (NPC) cells and tumor tissues, and re-expression of *MIPOL1* induced tumor suppression. The aim of the current study is to further elucidate the functional tumor suppressive role of *MIPOL1*. In this study, with expanded sample size of different clinical stages of NPC tumor tissues, we further confirmed the down-regulation of *MIPOL1* in different cancer stages. *MIPOL1* re-expression down-regulated angiogenic factors and reduced phosphorylation of metastasis-associated proteins including AKT, p65,

and FAK. In addition, MIPOL1 was confirmed to interact with a tumor suppressor, RhoB, and re-expression of MIPOL1 enhanced RhoB activity. The functional role of MIPOL1 was further validated by utilizing a panel of wild type (WT) and truncated *MIPOL1* expression constructs. The *MIPOL1* tumor suppressive effect can only be observed in the WT *MIPOL1*-expressing cells. *In vitro* and nude mice *in vivo* functional studies further confirmed the critical role of WT *MIPOL1* in inhibiting migration, invasion, and metastasis in NPC. Overall, this study provides strong evidence about the tumor suppressive role of *MIPOL1* in inhibiting angiogenesis and metastasis in NPC.

Keywords:

MIPOL1; NPC; RhoB; angiogenesis; metastasis

Introduction:

Chromosome 14q deletion is generally linked to a variety of diseases including developmental delay, intellectual disability, behavioral problems, and distinctive facial features[1, 2]. In addition, chromosome 14 deletion can be detected in various cancer types, including nasopharyngeal carcinoma (NPC), early-onset colon cancer[3], and meningioma progression[4]. In our previous cancer study, a functional microcell-mediated chromosome transfer (MMCT) complementation approach was utilized to transfer an intact chromosome 14 into a tumorigenic cell line to investigate the relevant tumor suppressive ability during *in vivo* mouse tumor development[5]. This MMCT study identified a candidate tumor suppressor gene (TSG), *Mirror Image Polydactyly 1 (MIPOL1),* that maps within the 14q13.1-13.3 tumor suppressive critical region and showed significant tumor suppressive ability.

Mapped within a translocation breakpoint t(2;14)(p23.3;q13), *MIPOL1* was first identified in a developmental disease, Mirror-image polydactyly of hands and feet, a very rare congenital abnormality in which the patients are characterized as having mirror-image duplication of digits[6]. This breakpoint is located within the intron 11 of *MIPOL1*. In another study of a patient with mild craniofacial and callosal central nervous system midline defects, a translocation of *MIPOL1* was also identified[7]. Genetic variations in the *SSTR1-MIPOL1* and the *TSLP-SLC25A46* loci show associations with the age at onset of the allergic rhinitis[8]. In addition, the clinical significance of *MIPOL1* associated with different cancers was identified. A transcriptome sequencing study in prostate cancer showed the fusion of *MIPOL1* exon 11 with the last exon of *DGKB* gene[9]. In a recent lung cancer study, a 1.2 Mb chromosome 14q13.3 common deletion region that included the *MIPOL1* was detected in the tumors[10]. These studies support *MIPOL1* deletions contributing to some cancers.

Our previous study showed significant down-regulation of *MIPOL1* in NPC patient tumors is associated with promoter hypermethylation and loss of heterozygosity (LOH)[5]. At the functional level, re-expression of *MIPOL1* in tumorigenic cell lines was found to significantly suppress *in vivo* tumor growth[5]. Similar to the synovial fibroblasts of patients with rheumatoid arthritis[11], hypermethylation of the *MIPOL1* promoter region was also detected in NPC cell lines, as well as directly in clinical samples[5]. These results further support the tumor suppressive role of *MIPOL1*. However, the exact function of *MIPOL1* in cancer development remains unclear. Therefore, in the current studies, we aim to perform comprehensive MIPOL1 functional studies in order to elucidate its mechanisms in NPC development.

Materials and Methods:

Cell culture and cell lines:

HONE-1 (RRID:CVCL_8706), NPC/HK1 (RRID:CVCL_7084), and HEK293-FT (RRID:CVCL_6911) cell lines were cultured in DMEM with 5% fetal bovine serum (FBS) (GIBCO, Invitrogen, Carlsbad, CA), and 5% newborn calf serum (NCS) (GIBCO, Invitrogen, Carlsbad, CA). It has been shown that HONE-1 contains parts of the HeLa genome, suggesting that HONE-1 is a product of a somatic hybridization with HeLa cells [12]. HONE-1 was established from a 27-year-old Chinese man with poorly differentiated NPC and NPC/HK1 from a 41-year-old Chinese male with well-differentiated NPC[13, 14]. All the cell lines were obtained from the NPC Area of Excellence (AoE) Research Tissue Bank Cell Line Repository and have been authenticated using STR profiling within the last three years. All the experiments were performed with mycoplasma-free cells.

Clinical samples:

Matched tumor and non-tumor archived frozen biopsy specimens from 119 NPC patients were obtained from the NPC AoE Research Tissue Bank with written consent from patients. In brief, the NPC tumor tissues were homogenized and the total RNA was collected by using TRIzol reagent (Invitrogen, CA, USA). The total RNA was subsequently converted to cDNA using Moloney Murine Leukemia Virus (M-MLV) reverse transcriptase (USB, Cleveland, Ohio, USA) according to the manufacturer's protocol.

Yeast two-hybrid (Y2H) assay:

The Y2H assay was performed according to the product insert from Matchmarker® Gold Yeast Two-Hybrid System (Takara Bio, USA). The RhoB and MIPOL1 full-length constructs were cloned into the vector, pGADT7 and pGBKT7. The vectors were transformed into yeast strain AH109 by electroporation methods. After transformation, the AH109 cells were selected in 2 drop-out medium (without leucine and tryptophan) to select pGADT7 and pGBKT7 positive clones. The positive clones were then sub-cultured on a 4 drop-out plate (without adenine, histidine, leucine, and tryptophan) to confirm the interaction. The vector-alone and parental AH109 cells were used as negative control.

Protein array analysis:

The protein lysates from the previously established vector-alone (VA) and *MIPOL1*-expression HONE-1[5] were utilized for the angiogenesis protein array (Ray Biotech, Norcoss, GA, USA) and human phospho-kinase antibody array (R&D System, Minneapolis, MN, USA) according to the manufacturer, as described previously[15]. **Supplementary Table 1** lists the targets analyzed from the angiogenesis and phospho-kinase protein arrays. The results were quantified using ImageJ (National Institutes of Health, Bethesda, MD USA)[16].

Real-Time qPCR:

The gene expression levels were determined by using FastStart Universal SYBR Green mastermix (Roche Applied Science, Upper Bavaria, Germany) and the LightCycler 480 Real-Time PCR instrument (Roche Applied Science, Upper Bavaria, Germany). Glyceraldehyde 3-phosphate dehydrogenase (GAPDH) was used as a housekeeping gene internal control to normalize the expression. Each reaction was repeated in triplicate and

the relative quantity of gene expression against the housekeeping gene control was calculated by $2^{-\Delta\Delta Ct}$. When the fold difference is greater than two-fold, the expression was considered to be significantly down-regulated.

Western blot analysis:

Western blot was performed in biological duplicates, as previously described[5]. The antibodies include MIPOL1 (1:1000; Sigma Aldrich, St. Louis, MO, USA), RhoB (1:1000; Genetex, Irvine, CA, USA), phospho-AKT (1:1000; Cell Signaling, Danvers, MA, USA), phospho-FAK (1:1000; Cell Signaling, Danvers, MA, USA), phospho-p65 (1:1000; Cell Signaling, Danvers, MA, USA), and p84 (1:1000; Genetex, Irvine, CA, USA) was used as a loading control. Quantification of the bands was performed utilizing ImageJ (National Institutes of Health, Bethesda, MD USA)[16].

RhoB assay:

The RhoB activity was determined according to the RhoB Activation Assay Kit (STA-403-B; Cell Biolabs, San Diego, USA). The total input lysate was used as a loading control.

Co-immunoprecipitation assay:

The co-immunoprecipitation was performed according to the Pierce™ Classic Magnetic IP/Co-IP Kit (88804, Thermo Scientific, Rockford, USA). 10 μL of the lysate was used as the input control, and 8μg of IgG mouse and MIPOL1 antibody were used for negative control and immunoprecipitation, respectively.

Gene transfection and lentiviral infection:

The previously established wild type (WT) *MIPOL1* stable-expressing clones were used[5]. The *MIPOL1* WT and two truncation mutants, ΔN100 and ΔC200-442, were established and subcloned to pLVX-EF1α lentiviral expression vector (modified from pLVX-CMV; Clontech) in HONE-1 and NPC/HK1 as described[17].

2-Dimensional (2D) and 3-Dimensional (3D) colony formation assay:

The 2D and 3D colony formation assays were carried out, as previously described[18]. In 2D colony formation assays, 5000 cells were seeded onto 6-well plates in triplicate and allowed to grow for two weeks before fixing in 10% formalin (Sigma-Aldrich, St. Louis, MO, USA) and staining with 1X diluted Giemsa reagent (Sigma-Aldrich, St. Louis, MO, USA). A total of 2000 cells were seeded onto 96-well Matrigel (BD Biosciences, San Jose, CA, USA) coated plates for 3D colony formation assay. The microscopic views were captured after two weeks in culture and the total numbers of cell spheres, which grew with diameter over 100 μm, were counted.

Wound healing assay:

The wound healing assay was performed, as previously reported[17]. The percentage of wound closure was calculated by the formula: (migrated distance after 24 hour/initial distance of wound width) ×100.

Transwell migration and invasion assays:

The transwell migration and invasion assays were performed, as previously drescribed[17, 19]. In brief, 2×10^5 cells were seeded onto the migration and invasion chambers (BD Biosciences, San Jose, CA, USA) with serum-free medium. The bottom of the chambers

containing 10% serum-enriched medium served as a chemoattractant. The cells were cultured for 24 and 36 hours, for migration and invasion chambers, respectively, before termination and followed by staining with crystal violet. The images of the chambers were captured by a Cytation 5 imaging reader (BioTek, VT, USA) and quantified by ImageJ software (HNI, Bethesda, MD USA).

In vivo tumorigenicity and metastasis assays:

The *in vivo* tumorigenicity assay was performed as described previously[15]. In brief, 1×10^7 cells were injected subcutaneously to both flanks of three female nude mice (BALB/cAnN-nu) per group. The sizes of tumors were measured weekly. The study endpoints were when the tumor volume exceeded 1000 mm^3 or the tumor ulcerated. The *in vivo* metastasis assay was conducted by injecting 1×10^6 cells into the spleen of the mice, as previous described[15]. Upon intraperitoneal injection of D-luciferin, the bioluminescent signal was monitored weekly using the Xenogen IVIS 100 *in vivo* Imaging System in the Faculty Core Facility, University of Hong Kong. Three weeks after inoculation, the mice were sacrificed, and the spleens and livers were excised to examine the tumor metastasis. All the *in vivo* assays were carried out under the approval of an ethical committee from the Department of Health, HKSAR and in the Laboratory Animal Unit of the University of Hong Kong, which is accredited under the Associating for Assessment and Accreditation of Laboratory Animal Care (AAALAC) international guidelines.

Paraffin embedding and Hematoxylin and Eosin (H&E) staining:

The paraffin embedding and H&E staining were conducted as described[17].

Statistical analysis:

Student's t-test or Fisher's exact test was used for all the statistical analysis unless stated otherwise. A *p*-value less than 0.05 was considered statistically significant (*$p < 0.05$, **$p < 0.01$, ***$p < 0.001$). The error bars represent the standard error mean (S.E.M.).

Data availability statement:

The data that support the findings of this study are available from the corresponding author upon reasonable request.

Results:

MIPOL1 re-expression suppresses cancer-related signaling pathways

In order to investigate the tumor suppressive role of *MIPOL1*, the clinical significance was first examined in a panel of NPC tumor samples representing different clinical stages by utilizing qPCR. For the 119 NPC biopsies and their paired adjacent non-tumor tissues, 75% of the tumors showed more than two-fold down-regulation of *MIPOL1* compared to the matched non-tumor tissues, in all early and advanced stages of tumors. Specifically, the levels of *MIPOL1* from the patients in stages I to IV were decreased in 81% (13/16), 69% (18/26), 78% (38/49) and 71% (20/28) of the specimens, respectively, suggesting a clinical significance of down-regulation of *MIPOL1* **(Figure 1A, Supplementary Table 2)**.

After examining the clinical significance of *MIPOL1*, the functional role of *MIPOL1* in tumor suppression was further investigated. Our previous study showed that the expression of *MIPOL1* in HONE-1 and NPC/HK1 was significantly down-regulated compared with a nasopharyngeal epithelial cell line (NP69)[5]. Therefore, re-expression of *MIPOL1* in these two NPC cell lines was established[5]. Firstly, an angiogenesis protein array and human phospho-kinase antibody array were utilized to identify the signaling mechanisms that are

regulated by MIPOL1. A panel of key metastasis and pro-angiogenesis factors, including angiogenin, IL6, IL8, MCP1, PDGFBB, and TIMP-2 were significantly down-regulated, when *MIPOL1* was re-expressed **(Figure 1B, Supplementary Figure 1A)**. This result suggests *MIPOL1* re-expression may induce significant anti-metastasis and/or anti-angiogenesis effects. In addition, the human phospho-kinase antibody array was used to determine the changes of phosphorylation levels of cancer-associated kinases upon *MIPOL1* re-expression. Re-expression of *MIPOL1* induced the reduced phosphorylation levels of a panel of cancer-associated kinases, including Hck, TOR, FAK, ERK1/2, AKT, RSK1/2/3, eNOS, c-jun, Pyk2, PLCγ1, and Paxillin **(Figure 1C, Supplementary Figure 1B)**. Among these, the AKT signaling pathway is closely related to cancer cell migration, invasion, and metastasis[20-23]. This provided the hints for further study of the functional role of *MIPOL1*.

MIPOL1 protein interacts with tumor suppressor RhoB and enhances its cellular activity

As the functional role of MIPOL1 was still not well-characterized, its protein interacting partners were identified by a yeast-two-hybrid approach. RhoB was one of the candidates identified from our previous yeast two-hybrid screening to interact with MIPOL1. Also, RhoB was reported to be an important tumor suppressor limiting cell proliferation, survival, invasion, and metastasis[24]. Therefore, the interaction between RhoB and MIPOL1 was firstly validated. Co-transformation of bait and prey vectors containing *RhoB* and *MIPOL1* into yeast cells resulted in the growth of yeast cells on a high stringency 4 drop-out plate. This suggested there is a potential interaction between RhoB and MIPOL1 **(Figure 1D)**. The interaction of MIPOL1 and RhoB was further confirmed by co-immunoprecipitation (Co-IP) **(Figure 1E)**. Since RhoB was reported to regulate both cell migration and

invasion[25, 26], the possible role of MIPOL1 in regulating RhoB activity was further investigated. In order to study the function of MIPOL1, two MIPOL1 deletion constructs, ΔN100 and ΔC200-442, were established for downstream studies **(Figure 2A)**. The RhoB activity was tested by a RhoGTPase activation assay by pulling-down the activated RhoB with Rhotekin (RTKN). Re-expression of the *MIPOL1* WT in tumorigenic HONE-1 and NPC/HK1 cells showed an increased level of activated RhoB, while the ΔN100 and ΔC200-442 showed a decreased activated RhoB level, when compared to the WT construct **(Figure 2B, Supplementary Figure 2)**. Furthermore, the qPCR assay was used to validate the result from the angiogenesis array. The results are consistent with those in the angiogenesis protein array and further indicated that only the *MIPOL1* WT could inhibit the pro-angiogenic/metastasis factors expression, while the ΔN100 and ΔC200-442 constructs did not show the suppression of pro-angiogenic factors expression **(Figure 2C)**; this suggested the intact MIPOL1 is critical to suppress the angiogenesis. In addition, the phosphorylation levels of AKT, p65, and FAK, were also validated in the MIPOL1 WT and truncated construct-expressing clones **(Figure 2D, Supplementary Figure 3)**; the results are consistent with that re-expression of *MIPOL1* WT could reduce the phosphorylation of the members identified by the phosphorylation array.

Re-expression of MIPOL1 suppresses in vitro clonogenic survival, migration and invasion abilities

To further confirm the role of *MIPOL1* in suppressing the migration and invasion, 2D and 3D colony formation assays were performed to assess clonogenic survival ability of tumor cells, which is a prerequisite for occurrence of metastasis[27, 28]. From the 2D colony formation assay **(Figure 3A)**, the number of colonies formed with intact *MIPOL1* was

reduced to 20% and 40% only, for both tumorigenic cell lines, HONE-1 and NPC/HK1 respectively, compared to the vector-alone (VA) control. However, that of those with the two truncation forms were similar to their corresponding VA controls. The similar trend can be seen in the 3D colony formation assay **(Figure 3B)**, in which the cells were cultured on the 3D Matrigel matrix to mimic the extracellular matrix (ECM) environment. Compared with the VA, the formation of tumor spheres (≥ 100 μm) for HONE-1 and NPC/HK1 with intact *MIPOL1* expression was reduced to 60% and 30%, respectively. The results suggested that the intact *MIPOL1,* but not the two truncation forms, can inhibit the 2D and 3D colony formation in HONE-1 and NPC/HK1. Subsequently, we examined the ability of *MIPOL1* to inhibit *in vitro* migration in the wound healing assay. The results showed that re-expression of *MIPOL1* WT in both HONE-1 and NPC/HK1 caused a suppression of the cell motility **(Figure 4A)**. The reduction of migration and invasion abilities in HONE-1 and NPC/HK1 with *MIPOL1* WT re-expression was further validated by *in vitro* migration and invasion chamber assays **(Figure 4B)**. For the migration chamber assay, the relative migration ability for HONE-1-WT and NPC/HK1-WT is significantly suppressed to 70% and 30%, respectively, when compared with the VA controls. However, no significant changes can be seen in the other two truncation forms. Likewise, in the Matrigel-coated invasion chambers, the relative invasion abilities were also significantly lower in the *MIPOL1* WT expressing HONE-1 (70%) and NPC/HK1 (40%) compared with VA controls **(Figure 4B)**. These results confirm the functional role of *MIPOL1* WT in suppression of *in vitro* NPC cell migration and invasion.

Intact MIPOL1, but not the truncation forms, inhibits in vivo metastasis and tumor growth

The nude mouse animal model was used to determine the ability of *MIPOL1* to inhibit *in vivo* metastasis, as the *in vitro* results indicated that *MIPOL1* can regulate the migration and invasion ability in metastatic cells. A luciferase-labelled metastatic cell line, HONE-1-Luc, was used for intrasplenic (IS) injection in the nude mice **(Figure 5A)**. Obvious tumor metastasis to the liver regions was detected **(Figure 5B)** in the control group VA in 7 of 7 tumors, the *MIPOL1* truncation ΔN100 in all 4 livers, and the ΔC200-442 group in 8 of 8 livers, whereas only 17% of tumors from the *MIPOL1* WT group (3/19) contained visible tumors **(Figure 5C)**. The inhibition of the liver metastasis ability in the WT group compared with other groups is statistically significant (VA vs WT, $p = 0.0002$; ΔN100 vs WT, $p = 0.004$; and ΔC200-442 vs WT, $p = 0.0001$). The results were further validated by H&E staining, as shown in representative images of the spleen and liver **(Figure 5D)**. The tumor suppressive role of *MIPOL1* was also evaluated by the *in vivo* tumorigenicity assay. The results showed that the tumor growth from the subcutaneously injected HONE-1 and NPC/HK1 with *MIPOL1* WT were significantly inhibited compared with the VA, ΔN100, and ΔC200-442 **(Figure 5E)**. These *in vivo* studies suggest that the re-expression of *MIPOL1* WT is associated with inhibiting the tumor metastasis and tumor growth.

Discussion:

Our *in vitro* and *in vivo* studies provide strong evidence that intact *MIPOL1* could suppress expression of angiogenic factors, cell migration, invasion, and metastasis, likely via the enhanced RhoB activity. Firstly, we showed that *MIPOL1* is down-regulated in a panel of NPC tumor specimens through all cancer stages, suggesting the important tumor suppressive role of *MIPOL1* in different stages. Since re-expression of *MIPOL1* suppressed *in vivo* tumorigenesis and metastasis **(Figure 5)**, it suggested that down-regulation of

MIPOL1 promotes tumorigenesis, cell proliferation, and later contributes to tumor metastasis. As *MIPOL1* is down-regulated in NPC tumors, the down-regulation of *MIPOL1* is associated with elevation of the metastasis-related factors and, hence, promotes tumor metastasis. Our study showed that the metastasis-associated factors including angiogenin, IL6, IL8, and MCP1 were down-regulated, when *MIPOL1* was re-expressed, suggesting these angiogenic factors are involved in metastasis. A study showed that overexpression of *IL8* enhanced AKT activity and promoted migration and invasion in gastric cancer cells[29]. Similarly, another *in vitro* study showed that IL6 promoted migration and invasion activities in NPC[30]. In a clinical study, Jin *et al* showed that a number of cytokines, including IL6 and MCP1, are upregulated in NPC patients[31]. This confirmed the clinical significance of upregulation of the panel of pro-metastatic factors we identified. These studies are consistent with our results that, when *MIPOL1* was re-expressed, this panel of factors was down-regulated and, thereby, suppressed the migration, invasion, and metastasis.

Our studies also showed that the RhoB activity was enhanced, when *MIPOL1* was re-expressed, and RhoB could interact with MIPOL1. In fact, RhoB was reported to play an important tumor suppressive role in different cancers including thyroid[32], brain[33], and lung cancers[34, 35], and invasive head and neck cancers[36] by promoting anti-proliferation and apoptosis[24]. Also, RhoB was reported to control the AKT trafficking during vascular development and has anti-metastasis activities[25, 37, 38]. Furthermore, loss of RhoB expression promoting migration and invasion by activating AKT was reported[26]. In an anti-cancer drug study, a citrus flavonoid, nobiletin, suppressed migration and invasion in gastric adenocarcinoma cells by up-regulation of the RhoB and inhibition of the

FAK/PI3K/AKT pathway[39]. In our study, as RhoB was activated, while the phospho-AKT and phospho-FAK were suppressed upon re-expression of *MIPOL1*, it is likely that *MIPOL1* down-regulates phospho-AKT and phospho-FAK through activating RhoB, resulting in inhibition of migration, invasion, and metastasis. Whether the activation of RhoB in NPC is due to the interaction with MIPOL1 needs further investigation.

Matrix metalloproteinases (MMPs) are a group of zinc-dependent extracellular matrix (ECM)-degrading enzymes highly associated with tumor cell invasion[40]. Moreover, it is well-established that a transcription factor, nuclear factor-κB (NF-κB), binds to the promoter region of MMP-9 and, hence, promotes its expression[41]. Interestingly, AKT was reported to induce MMP9 via activation of NF-κB transcription activity[42]. In fact, activation of NF-κB through AKT to increase transcription of a variety of genes has been widely reported[43, 44]. In our results, we also showed that re-expression of *MIPOL1* is associated with suppression phosphorylation of AKT and p65, a subunit of NF-κB. This suggests that *MIPOL1* may inhibit invasion by suppression of phosphorylation of AKT and p65 to further inhibit the expression of MMP-9. In addition, since the pro-angiogenic candidates we identified, including IL6 and IL8, are the targets of a transcription factor NF-κB[45], it is possible that re-expression of *MIPOL1* suppresses phospho-p65 to regulate the expression of *IL6* and *IL8.*

However, one limitation in this study is that the cell lines used, HONE-1 and NPC/HK1, are Epstein-Barr Virus (EBV)-negative. Since the majority of NPC cases are EBV-positive, more functional studies extending to other EBV-positive NPC cell lines, such as C666-1 and NPC43, would be useful to support a functional role of *MIPOL1* in NPC. Another limitation is that the NPC biopsies are characteristically heavily infiltrated with

lymphocytes and inflammatory stroma[46]. Due to the small sizes of biopsies obtained from patients, routine histopathological examination could not be performed to ascertain the % carcinoma content of the NPC tumor biopsies. This innate NPC tumor heterogeneity could affect overall results. The qPCR results **(Figure 1A, Supplementary Table 2)** showed that the expression of *MIPOL1* is generally down-regulated in the NPC tumors compared to their matched non-tumor tissues. In addition, our functional studies also support the down-regulation of *MIPOL1* in NPC cell lines, suggesting the general down-regulation of *MIPOL1* in NPC tumors associated with the functional effects.

In conclusion, the current study highlights the tumor suppressive role of *MIPOL1* in inhibiting migration, invasion, metastasis, and tumor growth via suppressing the expression and phosphorylation of cancer-related pathways. MIPOL1 was demonstrated to interact with a tumor suppressor, RhoB, and enhance the RhoB activity. The consistent loss of function of the two truncation forms of *MIPOL1* from our *in vitro* and *in vivo* studies strongly supports the conclusion that re-expression of intact *MIPOL1* is essential for its tumor suppressive role.

Acknowledgments:

This project was supported by the Research Grants Council of the Hong Kong Special Administrative Region, People's Republic of China: Grant number 17101715 to AKLC and MLL. We also acknowledge the NPC Area of Excellence (AoE) Tissue Bank for providing tissues for examining the expression level of *MIPOL1*.

The authors declare no conflict of interest.

References:

1. Petek E, Plecko-Startinig B, Windpassinger C, Egger H, Wagner K, Kroisel PM. Molecular characterisation of a 3.5 Mb interstitial 14q deletion in a child with several phenotypic anomalies. *J Med Genet* 2003;**40**: e47.

2. Schlade-Bartusiak K, Ardinger H, Cox DW. A child with terminal 14q deletion syndrome: consideration of genotype-phenotype correlations. *Am J Med Genet A* 2009;**149A**: 1012-8.

3. Mourra N, Zeitoun G, Buecher B, Finetti P, Lagarde A, Adelaide J, Birnbaum D, Thomas G, Olschwang S. High frequency of chromosome 14 deletion in early-onset colon cancer. *Dis Colon Rectum* 2007;**50**: 1881-6.

4. Simon M, von Deimling A, Larson JJ, Wellenreuther R, Kaskel P, Waha A, Warnick RE, Tew JM, Jr., Menon AG. Allelic losses on chromosomes 14, 10, and 1 in atypical and malignant meningiomas: a genetic model of meningioma progression. *Cancer Res* 1995;**55**: 4696-701.

5. Cheung AK, Lung HL, Ko JM, Cheng Y, Stanbridge EJ, Zabarovsky ER, Nicholls JM, Chua D, Tsao SW, Guan XY, Lung ML. Chromosome 14 transfer and functional studies identify a candidate tumor suppressor gene, mirror image polydactyly 1, in nasopharyngeal carcinoma. *Proc Natl Acad Sci U S A* 2009;**106**: 14478-83.

6. Kondoh S, Sugawara H, Harada N, Matsumoto N, Ohashi H, Sato M, Kantaputra PN, Ogino T, Tomita H, Ohta T, Kishino T, Fukushima Y, et al. A novel gene is disrupted at a 14q13 breakpoint of t(2;14) in a patient with mirror-image polydactyly of hands and feet. *J Hum Genet* 2002;**47**: 136-9.

7. Kamnasaran D, O'Brien PC, Zackai EH, Muenke M, Ferguson-Smith MA, Cox DW. Rearrangement in the PITX2 and MIPOL1 genes in a patient with a t(4;14) chromosome. *Eur J Hum Genet* 2003;**11**: 315-24.

8. Nilsson D, Henmyr V, Hallden C, Sall T, Kull I, Wickman M, Melen E, Cardell LO. Replication of genomewide associations with allergic sensitization and allergic rhinitis. *Allergy* 2014;**69**: 1506-14.

9. Maher CA, Kumar-Sinha C, Cao X, Kalyana-Sundaram S, Han B, Jing X, Sam L, Barrette T, Palanisamy N, Chinnaiyan AM. Transcriptome sequencing to detect gene fusions in cancer. *Nature* 2009;**458**: 97-101.

10. Harris T, Pan Q, Sironi J, Lutz D, Tian J, Sapkar J, Perez-Soler R, Keller S, Locker J. Both gene amplification and allelic loss occur at 14q13.3 in lung cancer. *Clin Cancer Res* 2011;**17**: 690-9.

11. Park SH, Kim SK, Choe JY, Moon Y, An S, Park MJ, Kim DS. Hypermethylation of EBF3 and IRX1 genes in synovial fibroblasts of patients with rheumatoid arthritis. *Mol Cells* 2013;**35**: 298-304.

12. Strong MJ, Baddoo M, Nanbo A, Xu M, Puetter A, Lin Z. Comprehensive high-throughput RNA sequencing analysis reveals contamination of multiple nasopharyngeal carcinoma cell lines with HeLa cell genomes. *J Virol* 2014;**88**: 10696-704.

13. Glaser R, Zhang HY, Yao KT, Zhu HC, Wang FX, Li GY, Wen DS, Li YP. Two epithelial tumor cell lines (HNE-1 and HONE-1) latently infected with Epstein-Barr virus that were derived from nasopharyngeal carcinomas. *Proc Natl Acad Sci U S A* 1989;**86**: 9524-8.

14. Huang D, Ho J, Poon Y, Chew E, Saw D, Lui M, Li C, Mak L, Lai S, Lau W. Establishment of a cell line (NPC/HK1) from a differentiated squamous carcinoma of the nasopharynx. *International journal of cancer* 1980;**26**: 127-32.

15. Cheung AK, Ip JC, Chu AC, Cheng Y, Leong MM, Ko JM, Shuen WH, Lung HL, Lung ML. PTPRG suppresses tumor growth and invasion via inhibition of Akt signaling in nasopharyngeal carcinoma. *Oncotarget* 2015;**6**: 13434-47.

16. Schneider CA, Rasband WS, Eliceiri KW. NIH Image to ImageJ: 25 years of image analysis. *Nat Methods* 2012;**9**: 671-5.

17. Chai AW, Cheung AK, Dai W, Ko JM, Ip JC, Chan KW, Kwong DL, Ng WT, Lee AW, Ngan RK, Yau CC, Tung SY, et al. Metastasis-suppressing NID2, an epigenetically-silenced gene, in the pathogenesis of nasopharyngeal carcinoma and esophageal squamous cell carcinoma. *Oncotarget* 2016;**7**: 78859-71.

18. Kan R, Shuen WH, Lung HL, Cheung AK, Dai W, Kwong DL, Ng WT, Lee AW, Yau CC, Ngan RK, Tung SY, Lung ML. NF-kappaB p65 Subunit Is Modulated by Latent Transforming Growth Factor-beta Binding Protein 2 (LTBP2) in Nasopharyngeal Carcinoma HONE1 and HK1 Cells. *PLoS One* 2015;**10**: e0127239.

19. Lung HL, Cheung AK, Cheng Y, Kwong FM, Lo PH, Law EW, Chua D, Zabarovsky ER, Wang N, Tsao SW, Stanbridge EJ, Lung ML. Functional characterization of THY1 as a tumor suppressor gene with antiinvasive activity in nasopharyngeal carcinoma. *Int J Cancer* 2010;**127**: 304-12.

20. Webb DJ, Donais K, Whitmore LA, Thomas SM, Turner CE, Parsons JT, Horwitz AF. FAK-Src signalling through paxillin, ERK and MLCK regulates adhesion disassembly. *Nat Cell Biol* 2004;**6**: 154-61.

21. Teranishi S, Kimura K, Nishida T. Role of formation of an ERK-FAK-paxillin complex in migration of human corneal epithelial cells during wound closure in vitro. *Invest Ophthalmol Vis Sci* 2009;**50**: 5646-52.

22. Mitra SK, Schlaepfer DD. Integrin-regulated FAK-Src signaling in normal and cancer cells. *Curr Opin Cell Biol* 2006;**18**: 516-23.

23. Chin YR, Toker A. Function of Akt/PKB signaling to cell motility, invasion and the tumor stroma in cancer. *Cell Signal* 2009;**21**: 470-6.

24. Huang M, Prendergast GC. RhoB in cancer suppression. *Histol Histopathol* 2006;**21**: 213-8.

25. Jiang K, Sun J, Cheng J, Djeu JY, Wei S, Sebti S. Akt mediates Ras downregulation of RhoB, a suppressor of transformation, invasion, and metastasis. *Mol Cell Biol* 2004;**24**: 5565-76.

26. Bousquet E, Mazieres J, Privat M, Rizzati V, Casanova A, Ledoux A, Mery E, Couderc B, Favre G, Pradines A. Loss of RhoB expression promotes migration and invasion of human bronchial cells via activation of AKT1. *Cancer Res* 2009;**69**: 6092-9.

27. Valastyan S, Weinberg RA. Tumor metastasis: molecular insights and evolving paradigms. *Cell* 2011;**147**: 275-92.

28. Franken NA, Rodermond HM, Stap J, Haveman J, van Bree C. Clonogenic assay of cells in vitro. *Nat Protoc* 2006;**1**: 2315-9.

29. Kuai WX, Wang Q, Yang XZ, Zhao Y, Yu R, Tang XJ. Interleukin-8 associates with adhesion, migration, invasion and chemosensitivity of human gastric cancer cells. *World J Gastroenterol* 2012;**18**: 979-85.

30. Sun W, Liu DB, Li WW, Zhang LL, Long GX, Wang JF, Mei Q, Hu GQ. Interleukin-6 promotes the migration and invasion of nasopharyngeal carcinoma cell lines and upregulates the expression of MMP-2 and MMP-9. *Int J Oncol* 2014;**44**: 1551-60.

31. Jin YB, Zhang GY, Lin KR, Chen XP, Cui JH, Wang YJ, Luo W. Changes of plasma cytokines and chemokines expression level in nasopharyngeal carcinoma patients after treatment with definitive intensity-modulated radiotherapy (IMRT). *PLoS One* 2017;**12**: e0172264.

32. Marlow LA, Reynolds LA, Cleland AS, Cooper SJ, Gumz ML, Kurakata S, Fujiwara K, Zhang Y, Sebo T, Grant C, McIver B, Wadsworth JT, et al. Reactivation of suppressed RhoB is a critical step for the inhibition of anaplastic thyroid cancer growth. *Cancer Res* 2009;**69**: 1536-44.

33. Forget MA, Desrosiers RR, Del M, Moumdjian R, Shedid D, Berthelet F, Beliveau R. The expression of rho proteins decreases with human brain tumor progression: potential tumor markers. *Clin Exp Metastasis* 2002;**19**: 9-15.

34. Mazieres J, Antonia T, Daste G, Muro-Cacho C, Berchery D, Tillement V, Pradines A, Sebti S, Favre G. Loss of RhoB expression in human lung cancer progression. *Clin Cancer Res* 2004;**10**: 2742-50.

35. Mazieres J, Tovar D, He B, Nieto-Acosta J, Marty-Detraves C, Clanet C, Pradines A, Jablons D, Favre G. Epigenetic regulation of RhoB loss of expression in lung cancer. *BMC Cancer* 2007;**7**: 220.

36. Adnane J, Muro-Cacho C, Mathews L, Sebti SM, Munoz-Antonia T. Suppression of rho B expression in invasive carcinoma from head and neck cancer patients. *Clin Cancer Res* 2002;**8**: 2225-32.

37. Adini I, Rabinovitz I, Sun JF, Prendergast GC, Benjamin LE. RhoB controls Akt trafficking and stage-specific survival of endothelial cells during vascular development. *Genes Dev* 2003;**17**: 2721-32.

38. Chen W, Niu S, Ma X, Zhang P, Gao Y, Fan Y, Pang H, Gong H, Shen D, Gu L, Zhang Y, Zhang X. RhoB Acts as a Tumor Suppressor That Inhibits Malignancy of Clear Cell Renal Cell Carcinoma. *PLoS One* 2016;**11**: e0157599.

39. Lee YC, Cheng TH, Lee JS, Chen JH, Liao YC, Fong Y, Wu CH, Shih YW. Nobiletin, a citrus flavonoid, suppresses invasion and migration involving FAK/PI3K/Akt and small GTPase signals in human gastric adenocarcinoma AGS cells. *Mol Cell Biochem* 2011;**347**: 103-15.

40. Stetler-Stevenson WG, Aznavoorian S, Liotta LA. Tumor cell interactions with the extracellular matrix during invasion and metastasis. *Annu Rev Cell Biol* 1993;**9**: 541-73.

41. Bond M, Fabunmi RP, Baker AH, Newby AC. Synergistic upregulation of metalloproteinase-9 by growth factors and inflammatory cytokines: an absolute requirement for transcription factor NF-kappa B. *FEBS Lett* 1998;**435**: 29-34.

42. Kim D, Kim S, Koh H, Yoon SO, Chung AS, Cho KS, Chung J. Akt/PKB promotes cancer cell invasion via increased motility and metalloproteinase production. *FASEB J* 2001;**15**: 1953-62.

43. Ozes ON, Mayo LD, Gustin JA, Pfeffer SR, Pfeffer LM, Donner DB. NF-kappaB activation by tumour necrosis factor requires the Akt serine-threonine kinase. *Nature* 1999;**401**: 82-5.

44. Romashkova JA, Makarov SS. NF-kappaB is a target of AKT in anti-apoptotic PDGF signalling. *Nature* 1999;**401**: 86-90.

45. Kim JW, Jang SM, Kim CH, An JH, Kang EJ, Choi KH. New molecular bridge between RelA/p65 and NF-kappaB target genes via histone acetyltransferase TIP60 cofactor. *J Biol Chem* 2012;**287**: 7780-91.

46. Tsao SW, Tsang CM, Lo KW. Epstein-Barr virus infection and nasopharyngeal carcinoma. *Philos Trans R Soc Lond B Biol Sci* 2017;**372**.

Figure legends:

Figure 1: Alteration of the cancer-related molecular signaling pathways contributed by *MIPOL1* and interaction of RhoB and MIPOL1. (A) qPCR analysis showed that expression of *MIPOL1* is more than two-fold down-regulated in 75% (89/119) of NPC biopsies. (B) Angiogenesis array to investigate the changes of angiogenesis-related protein in *MIPOL1*-expressing clone conditioned medium. The targets with significant changes are circled. (C) Phosphorylation array to investigate the changes of phosphorylation status of important kinases in the *MIPOL1*-expressing clone. The targets with significant changes are circled. (D) Interaction of MIPOL1 and RhoB confirmed by Y2H experiments. Interaction of MIPOL1 and RhoB was validated by observing the growth of the yeast cells on the 4-dropout plate. (E) Co-IP assay was performed by utilizing the antibodies against MIPOL1 and RhoB. The IgG was used as a negative control. MIPOL1 showed interaction with the RhoB in the HEK293-FT cell line.

Figure 2: Re-expression of wild type and truncated *MIPOL1* showing the association of *MIPOL1* expression with enhanced RhoB activity and suppressed the cancer-related signaling members. (A) A schematic diagram shows the protein conserved domains of *MIPOL1* WT and the deletion constructs (ΔN100: deletion of 1-100 amino acids (a.a) at N terminus; ΔC200-442: deletion of 200-442 a.a. at C terminus). (B) RhoB assay was used to study the RhoB activity by pulling-down the active RhoB with RTKN. *MIPOL1* WT in the NPC cell lines elevated RhoB activity, when compared to the VA control. The total RhoB was used as an equal loading control. (C) qPCR validated the down-regulation of some of the angiogenic factors, angiogenin, IL6, IL8, and MCP1, identified from the angiogenesis array in *MIPOL1*-re-expressing HONE-1 and NPC/HK1. The results also

showed that the expression of the deletion constructs was not able to suppress the angiogenic factors. (D) Re-expression of *MIPOL1* WT suppressed the phosphorylation of AKT, p65, and FAK in HONE-1 and NPC/HK1. The equal loading control was p84.

Figure 3: WT *MIPOL1* inhibits 2D and 3D colony formation. (A) 2D colony formation assays of HONE-1 and NPC/HK1 show that re-expression of *MIPOL1* WT can inhibit clonogenic survival. (B) In 3D colony formation assays, cells were seeded on a thin layer of Matrigel coated on the culture dish and the re-expression of *MIPOL1* WT in HONE-1 and NPC/HK1 contributed significantly to the reduction of colony-forming abilities. * indicates $p < 0.05$, ** indicates $p < 0.01$, and *** indicates $p < 0.001$. Data shown are the mean from three independent experiments with ± S.E.M as error bars.

Figure 4: *MIPOL1* WT suppresses *in vitro* cell migration and invasion. (A) Wound healing analysis was utilized to evaluate the cell migration ability. The reduced relative migration ability in the HONE-1-WT and NPC/HK1-WT can be seen 18 hours after the scratch. (B) *In vitro* chamber migration and invasion abilities were examined. Re-expression of *MIPOL1* WT in HONE-1 and NPC/HK1 significantly reduced the relative migration and invasion abilities compared with the VA control, but the relevant effects in the cells with ΔN100 and ΔC200-442 expression are not significant. * indicates $p < 0.05$, ** indicates $p < 0.01$, and *** indicates $p < 0.001$. Data shown are the mean from three independent experiments with ± S.E.M as error bars.

Figure 5: *MIPOL1* WT suppresses *in vivo* metastasis and NPC tumor growth. (A) Representative images of the Xenogen *in vivo* imaging system demonstrates the metastasis of the tumor from the spleen to the liver. (B) The livers from the sacrificed mice were

collected and the representative images show tumor lesions in the liver, indicated by the arrows. No observable tumors were found in the WT group. (C) The bar chart summarizes the liver metastasis ability for different groups of the mice. The percentages for VA, ΔN100, and ΔC200-442 are considerably higher compared with WT. This is statistically significant. (D) The excised livers and spleens were processed for histological examination. The representative H&E staining images show the presence of tumor in the spleens for all groups. For the H&E images from the livers, however, no observable tumor can be seen in the WT group. (E) Subcutaneous injection to the nude mice was used to assess the tumorigenicity by the *MIPOL1* WT, the two truncation constructs, and the VA control. The study endpoints for the HONE-1 and NPC/HK1 groups were three and four weeks, respectively. The result shows that the tumor growth was significantly inhibited in HONE-1 and NPC/HK1, when *MIPOL1* WT was re-expressed. This was not the case for VA, ΔN100 and ΔC200-442. ** indicates $p < 0.01$, and *** indicates $p < 0.001$.

Figure 1:

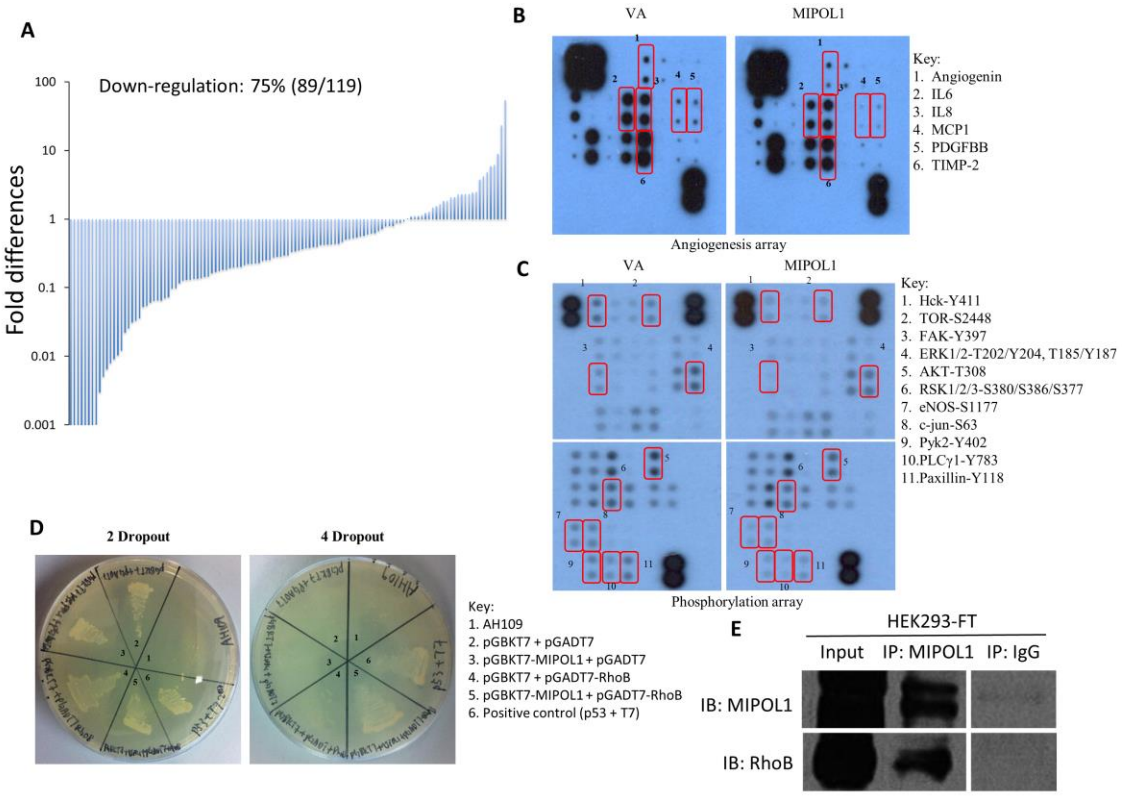
A
Down-regulation: 75% (89/119)
Fold differences
100
10
1
0.1
0.01
0.001
B
VA
MIPOL1
Key:
1. Angiogenin
2. IL6
3. IL8
4. MCP1
5. PDGFBB
6. TIMP-2
Angiogenesis array
C
VA
MIPOL1
Key:
1. Hck-Y411
2. TOR-S2448
3. FAK-Y397
4. ERK1/2-T202/Y204, T185/Y187
5. AKT-T308
6. RSK1/2/3-S380/S386/S377
7. eNOS-S1177
8. c-jun-S63
9. Pyk2-Y402
10.PLCγ1-Y783
11.Paxillin-Y118
Phosphorylation array
D
2 Dropout
4 Dropout
Key:
1. AH109
2. pGBKT7 + pGADT7
3. pGBKT7-MIPOL1 + pGADT7
4. pGBKT7 + pGADT7-RhoB
5. pGBKT7-MIPOL1 + pGADT7-RhoB
6. Positive control (p53 + T7)
E
HEK293-FT
Input
IP: MIPOL1
IP: IgG
IB: MIPOL1
IB: RhoB

Figure 2:

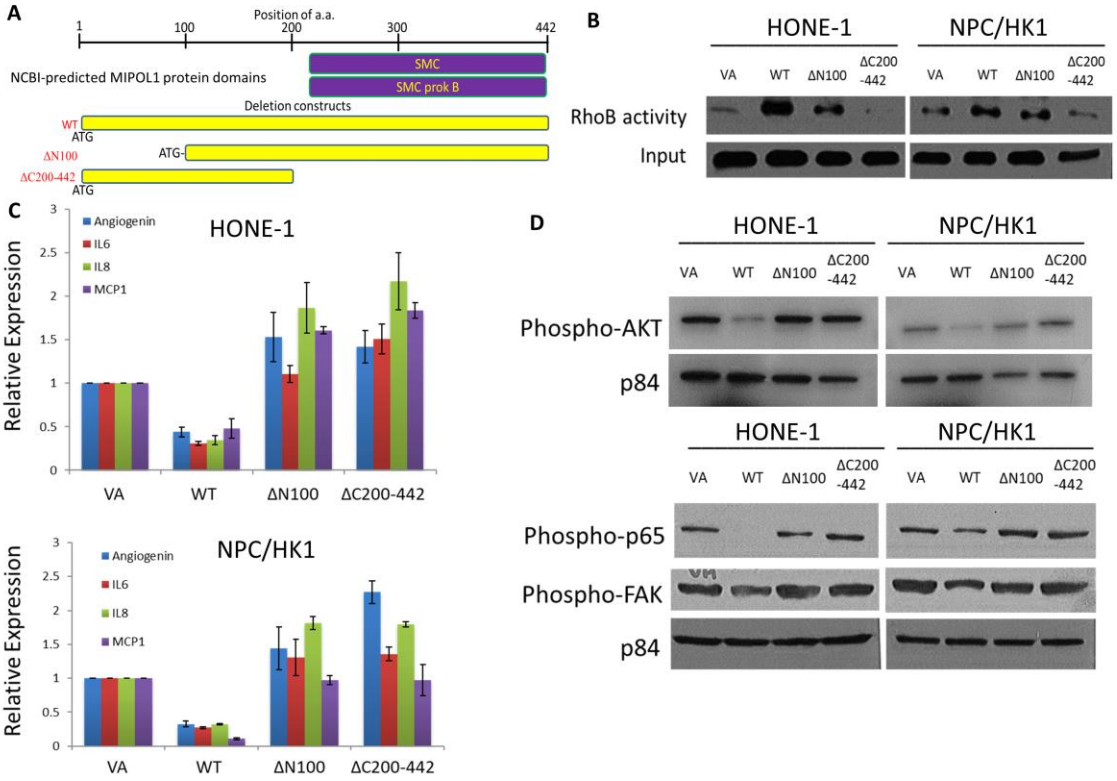
A
Position of a.a.
1
100
200
300
442
NCBI-predicted MIPOL1 protein domains
SMC
SMC prok B
Deletion constructs
WT
ATG
ΔN100
ATG-
ΔC200-442
ATG
B
HONE-1
NPC/HK1
VA
WT
ΔN100
ΔC200 -442
RhoB activity
Input
C
HONE-1
Angiogenin
IL6
IL8
MCP1
Relative Expression
VA
WT
ΔN100
ΔC200-442
NPC/HK1
D
HONE-1
NPC/HK1
Phospho-AKT
p84
Phospho-p65
Phospho-FAK
p84

Figure 3:

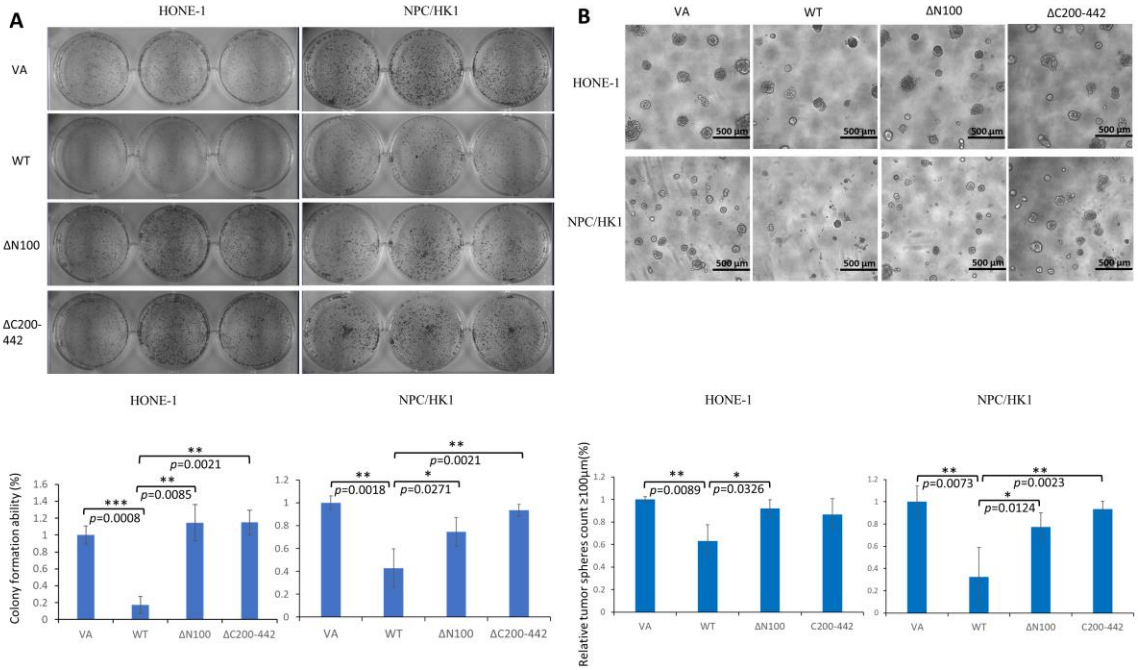
A
HONE-1
NPC/HK1
VA
WT
ΔN100
ΔC200-442
B
VA
WT
ΔN100
ΔC200-442
HONE-1
NPC/HK1
500 μm
HONE-1
NPC/HK1
Colony formation ability (%)
p=0.0008
p=0.0085
p=0.0021
p=0.0018
p=0.0271
p=0.0021
VA
WT
ΔN100
ΔC200-442
HONE-1
NPC/HK1
Relative tumor spheres count ≥100μm(%)
p=0.0089
p=0.0326
p=0.0073
p=0.0124
p=0.0023
VA
WT
ΔN100
C200-442

Figure 4:

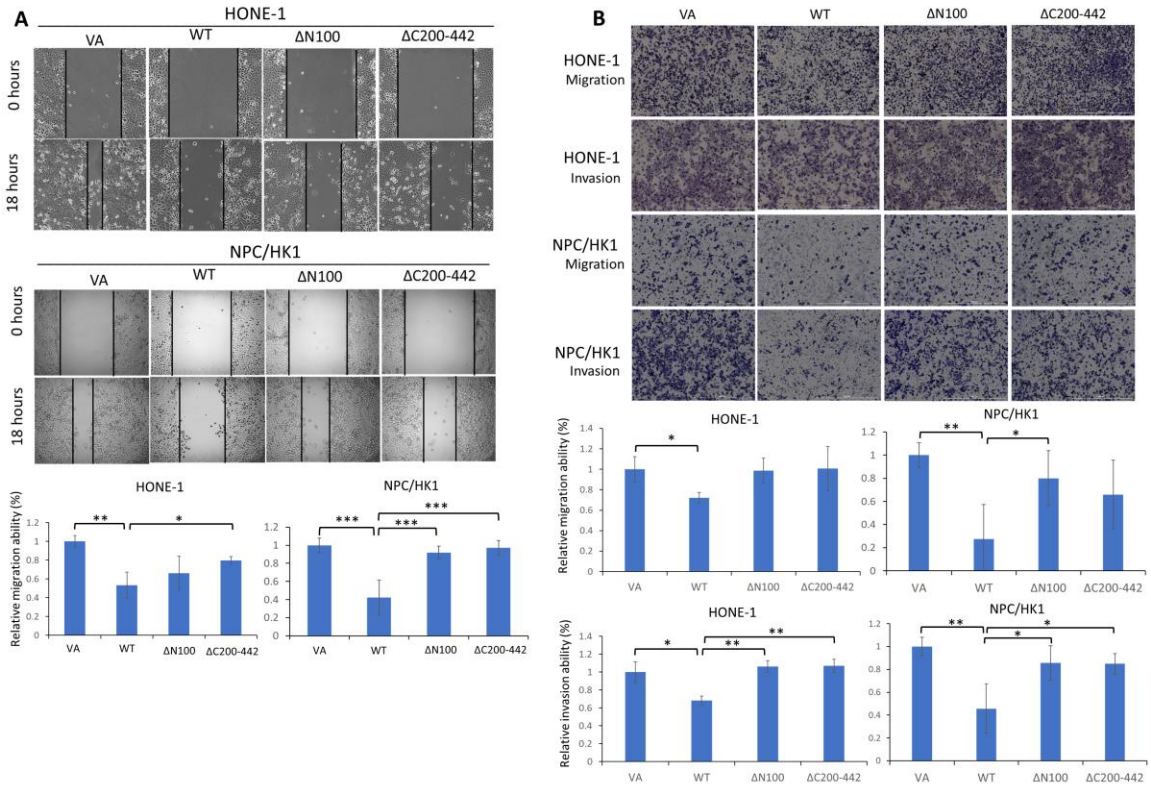
A
HONE-1
VA
WT
ΔN100
ΔC200-442
0 hours
18 hours
NPC/HK1
Relative migration ability (%)
B
HONE-1 Migration
HONE-1 Invasion
NPC/HK1 Migration
NPC/HK1 Invasion
Relative invasion ability (%)

Figure 5:

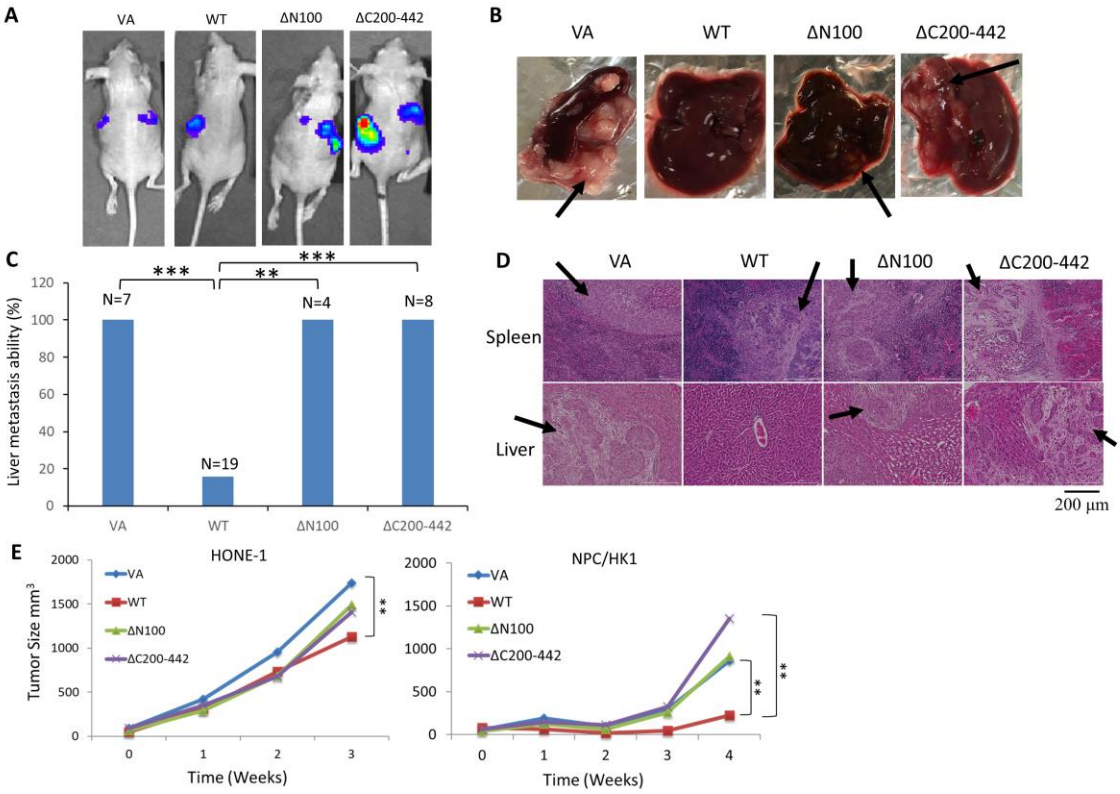
A
VA
WT
ΔN100
ΔC200-442
B
VA
WT
ΔN100
ΔC200-442
C
Liver metastasis ability (%)
***
***
**
N=7
N=19
N=4
N=8
VA
WT
ΔN100
ΔC200-442
D
VA
WT
ΔN100
ΔC200-442
Spleen
Liver
200 μm
E
HONE-1
NPC/HK1
Tumor Size mm3
VA
WT
ΔN100
ΔC200-442
Time (Weeks)
Time (Weeks)